CSMA 2024
16ème Colloque National en Calcul des Structures
13-17 Mai 2024, Presqu'île de Giens (Var)

Impact of morphological and crystallographic textures on the formability limits of thin metal sheets using a CPFEM-based approach

S. Zhou[1,2], M. Ben Bettaieb[1,2], F. Abed-Meraim[1,2]

[1] *Université de Lorraine, CNRS, Arts et Métiers Institute of Technology, LEM3, F-57070 Metz, France, {shuai.zhou, mohamed.benbettaieb, farid.abed-meraim}@ensam.eu*
[2] *DAMAS, Laboratory of Excellence on Design of Alloy Metals for low-mAss Structures, Université de Lorraine, France*

Abstract — The objective of this contribution is to investigate the influence of morphological and crystallographic textures on the formability limits of polycrystalline aggregates using the Crystal Plasticity Finite Element Method (CPFEM). The overall behavior of these polycrystalline aggregates is derived from that of the constituent single crystals by the periodic homogenization technique. The single crystal behavior is modeled by a rate-independent finite strain formulation, with the plastic flow rule governed by the classical Schmid law. Ultimately, the prediction of the formability limits is achieved by applying the Rice bifurcation criterion.
Keywords — Crystal plasticity, periodic homogenization, formability.

1 Introduction

Understanding the influence of relevant microstructural parameters on the ductility limits is essential for metallurgists and designers aiming to enhance the quality of their final products. Ductility is often limited by the incipience of various physical phenomena, such as plastic strain localization or void coalescence, which can occur simultaneously or separately. In the present investigation, attention is focused on the prediction of the onset of plastic strain localization, assumed to be the primary limiting factor affecting ductility. To predict such a phenomenon, several numerical tools have been developed in the past. In this field, various phenomenological and multiscale frameworks are commonly coupled with some localization criteria to predict the formability limits, following the concept of forming limit diagrams (FLDs). Despite their computational efficiency and ease of numerical implementation, phenomenological models are often unable to adequately capture the influence on the FLDs of some relevant microstructural phenomena, such as grain morphology, crystallographic texture, and grain boundary. To overcome these limitations, several multiscale schemes have been adopted for predicting the formability of thin metal sheets. Within these multiscale frameworks, the mechanical behavior is explicitly modeled at the single crystal scale, and some relevant scale-transition rules are used to obtain the macroscopic behavior from that of the microscopic constituents. The full-constraint Taylor scheme has been frequently used in FLD predictions, incorporating both rate-dependent [1] and rate-independent [2]-[4] frameworks to model the single crystal behavior. However, the Taylor model has inherent conceptual drawbacks, such as the failure to satisfy equilibrium conditions at the grain level and an inaccurate representation of grain morphology. To address these issues, the self-consistent multiscale scheme has found application in predicting the formability of thin metal sheets [2], [5], [6]. Despite their extensive use, both the Taylor and self-consistent multiscale schemes are often unable to accurately model the mechanical behavior of polycrystalline aggregates. To address some of the limitations of mean-field multiscale schemes (e.g. Taylor and self-consistent models), the full-field Crystal Plasticity Finite Element Method (CPFEM) has been proposed as a valuable tool for predicting forming limits. This method allows the consideration of strain heterogeneity within grains, originating from the collective motions of dislocations. It also incorporates realistic boundary conditions that accurately describe both geometric anisotropy and deformation-induced anisotropy, such as periodic boundary conditions. In the field of CPFEM applications, Amelirad and Assempour [7] have conducted a study exploring the impact of grain size on the forming limits of stainless steel 316 L sheets. More recently, Zhu et al. [3]-[4] have developed a new multiscale framework, based on the CPFEM, to predict the macroscopic behavior of polycrystalline ag-

gregates. In these latter studies, the CPFEM was coupled with the Rice bifurcation criterion [8] to predict the onset of plastic strain localization in polycrystalline aggregates. The computational tool developed in [3] and [4] is used in the present contribution to investigate the impact of morphological and crystallographic textures on the formability limits of thin metal sheets. Our findings align with several prior contributions in the literature, providing further insights into this critical area of materials science.

2 Constitutive Model

2.1 Single crystal constitutive equations

We consider an elastoplastic Face-Centered Cubic (FCC) single crystal subjected to an eulerian velocity gradient $\mathbf{g}$. In accordance with Mandel's theory, we assume the existence of an elastically relaxed configuration. The arbitrary rotation $\mathbf{r}$ of the relaxed configuration with respect to the current one is chosen so that the Schmid tensor $\bar{\mathbf{M}}^\alpha$ corresponding to slip system α remains constant over time. For FCC crystallographic structures, α ranges between 1 and 12. For clarity, any tensor presented in an orthonormal basis fixed with respect to these material orientations will be denoted by a superposed bar. Therefore, $\bar{\mathbf{g}} = \mathbf{r}^T \cdot \mathbf{g} \cdot \mathbf{r}$ represents the expression of $\mathbf{g}$ in this material basis, and $\bar{\mathbf{d}}$ and $\bar{\mathbf{w}}$ denote its symmetric and skew-symmetric parts, respectively. Under the small elastic strain assumption, tensors $\bar{\mathbf{d}}$ and $\bar{\mathbf{w}}$ can be additively decomposed into their elastic and plastic parts as follows:

$$\bar{\mathbf{d}} = \bar{\mathbf{d}}^e + \bar{\mathbf{d}}^p; \quad \bar{\mathbf{w}} = \bar{\mathbf{w}}^e + \bar{\mathbf{w}}^p. \tag{1}$$

In the present work, we assume linear and isotropic elastic behavior, which can be modeled by Hooke's law as follows:

$$\dot{\bar{\boldsymbol{\sigma}}} = \bar{\mathbf{c}}^e : \bar{\mathbf{d}}^e, \tag{2}$$

where $\bar{\mathbf{c}}^e$ is the fourth-order elastic stiffness tensor.

Plastic deformation is assumed to solely arise from crystallographic slip on the slip systems. Therefore, the plastic component of the velocity gradient $\bar{\mathbf{g}}$ can be defined as follows:

$$\bar{\mathbf{g}}^p = \bar{\mathbf{d}} + \bar{\mathbf{w}} = \sum_{\alpha=1}^{12} \dot{\gamma}^\alpha \bar{\mathbf{M}}^\alpha. \tag{3}$$

Here, $\dot{\gamma}^\alpha$ denotes the slip rate.

The plastic flow rule is defined by the classical Schmid law, which assumes that slip may occur only when the resolved shear stress τ^α on a specific slip system α attains a critical threshold τ_c^α:

$$\forall \alpha = 1, \cdots, 12 : \ |\tau^\alpha| \leq \tau_c^\alpha; \ (|\tau^\alpha| - \tau_c^\alpha)\, \dot{\gamma}^\alpha = 0. \tag{4}$$

The resolved shear stress τ^α is defined in terms of the Cauchy stress tensor $\bar{\sigma}$ and the symmetric part of the Schmid tensor $\bar{\mathbf{M}}^\alpha$ as follows:

$$\forall \alpha = 1, \cdots, 12 : \ \tau^\alpha = \bar{\boldsymbol{\sigma}} : \bar{\mathbf{M}}^\alpha_{sym}. \tag{5}$$

The evolution of the critical shear stress τ_c^α is governed by the following hardening law:

$$\forall \alpha = 1, \cdots, 12 : \ \dot{\tau}_c^\alpha = \sum_{\beta=1}^{12} H^{\alpha\beta} |\dot{\gamma}^\beta|. \tag{6}$$

In the current contribution, it is assumed that hardening is isotropic, and each component of the hardening interaction matrix $\mathbf{H}$ is determined by the following power law:

$$\forall \alpha = 1, \cdots, 12 : \ H^{\alpha\beta} = h_0 \left(1 + \frac{h_0 \Gamma}{\tau_0 n}\right)^{n-1}, \tag{7}$$

where h_0 and n represent hardening parameters, τ_0 denotes the initial critical shear stress, and Γ represents the accumulated slip, which is equal to $\sum_{\beta=1}^{12} |\dot{\gamma}^\beta|$.

2.2 Periodic homogenization equations

The periodic homogenization technique is used to determine the macroscopic behavior of the polycrystalline aggregates from the properties of their individual constituent single crystals. The rate form of the macroscopic nominal stress tensor $\dot{\mathbf{N}}$ and the macroscopic velocity gradient $\mathbf{G}$ are employed as appropriate work-conjugate variables. As in the majority of previous investigations, the macroscopic plane stress assumption is adopted for the prediction of forming limit diagrams. The in-plane part of a vector or tensor $\bullet$ is denoted ${}^{\mathrm{IN}}\bullet$. For brevity, only the main equations and steps of this technique are outlined in what follows, and more details can be found in [9].

- The macroscopic velocity gradient $\mathbf{G}$ and the rate of the macroscopic nominal stress tensor $\dot{\mathbf{N}}$ are related to their microscopic counterparts $\mathbf{g}$ and $\dot{\mathbf{n}}$ through the following averaging relations:
$$\mathbf{G} = \frac{1}{|\mathcal{V}|}\int_{\mathcal{V}} \mathbf{g}\, d\mathcal{V} \quad \text{and} \quad \dot{\mathbf{N}} = \frac{1}{|\mathcal{V}|}\int_{\mathcal{V}} \dot{\mathbf{n}}\, d\mathcal{V}, \tag{8}$$
where $\mathcal{V}$ is the current volume of the polycrystalline aggregate.
- The microscopic static equilibrium equation is expressed in terms of the rate of the microscopic nominal stress tensor $\dot{\mathbf{n}}$ as follows:
$$div_{\mathbf{x}}(\dot{\mathbf{n}}^T) = \mathbf{0}, \tag{9}$$
where $\mathbf{x}$ is the current position of the material point.
- The current in-plane velocity of a material point ${}^{\mathrm{IN}}\mathbf{v}$ is assumed to be linked the current in-plane position ${}^{\mathrm{IN}}\mathbf{x}$ and the in-plane part of the macroscopic velocity gradient ${}^{\mathrm{IN}}\mathbf{G}$ as:
$${}^{\mathrm{IN}}\mathbf{v} = {}^{\mathrm{IN}}\mathbf{G} \cdot {}^{\mathrm{IN}}\mathbf{x} + {}^{\mathrm{IN}}\mathbf{v}_{per}, \tag{10}$$
where ${}^{\mathrm{IN}}\mathbf{v}_{per}$ is an in-plane periodic velocity fluctuation field.
- The application of the periodic homogenization technique will be carried out by imposing the periodic conditions on the boundaries of the polycrystalline aggregates, as explained in [9].

3 Numerical Analysis

The constitutive equations at the single crystal scale are implemented within ABAQUS/Standard FE code through a user-defined material subroutine UMAT. To accurately represent the microstructure of the studied sheets, the polycrystalline aggregates used in the present contribution are composed of 125 grains. The effect of grain morphology on the ductility limits is investigated using three different grain shapes: cube, random and elongated, as shown in Figure 1a-1c. The different grain morphologies are generated by the NEPER software [10] on the basis of the Voronoi tessellation technique. The macroscopic loading is shown in Figure 1d. To be consistent with the classical FLD predictions, a macroscopic plane stress state is assumed in the Z direction ($\dot{N}_{33} = 0$). The polycrystalline aggregates are subjected to biaxial stretching in the X and Y directions, which is defined by strain ratio ρ as:

$$\rho = \frac{G_{22}}{G_{11}} = const. \tag{11}$$

where ρ ranges between -0.5 and 1 to span the complete FLDs. Then, in-plane tensors ${}^{\mathrm{IN}}\mathbf{G}$ and ${}^{\mathrm{IN}}\dot{\mathbf{N}}$ can be defined by the following generic forms:

$${}^{\mathrm{IN}}\mathbf{G} = \begin{pmatrix} G_{11} & 0 \\ 0 & \rho\, G_{11} \end{pmatrix}; \quad {}^{\mathrm{IN}}\dot{\mathbf{N}} = \begin{pmatrix} \dot{N}_{11} & \dot{N}_{12} \\ \dot{N}_{21} & \dot{N}_{22} \end{pmatrix}. \tag{12}$$

Tensors ${}^{\mathrm{IN}}\mathbf{G}$ and ${}^{\mathrm{IN}}\dot{\mathbf{N}}$ are related by the in-plane macroscopic tangent modulus ${}^{\mathrm{IN}}\mathbf{L}$:

$${}^{\mathrm{IN}}\dot{\mathbf{N}} = {}^{\mathrm{IN}}\mathbf{L} : {}^{\mathrm{IN}}\mathbf{G}, \tag{13}$$

with the macroscopic tangent modulus ${}^{\mathrm{IN}}\mathbf{L}$ determined using the condensation technique, as presented in [11].

To detect the occurrence of localized necking, the Rice bifurcation criterion [8] is used. This criterion states that strain localization occurs when the acoustic tensor $\vec{\mathcal{N}} \cdot {}^{\mathrm{IN}}\mathbf{L} \cdot \vec{\mathcal{N}}$ becomes singular and the corresponding determinant vanishes, which is given by:

$$\det\left(\vec{\mathcal{N}} \cdot {}^{\mathrm{IN}}\mathbf{L} \cdot \vec{\mathcal{N}}\right) = 0. \tag{14}$$

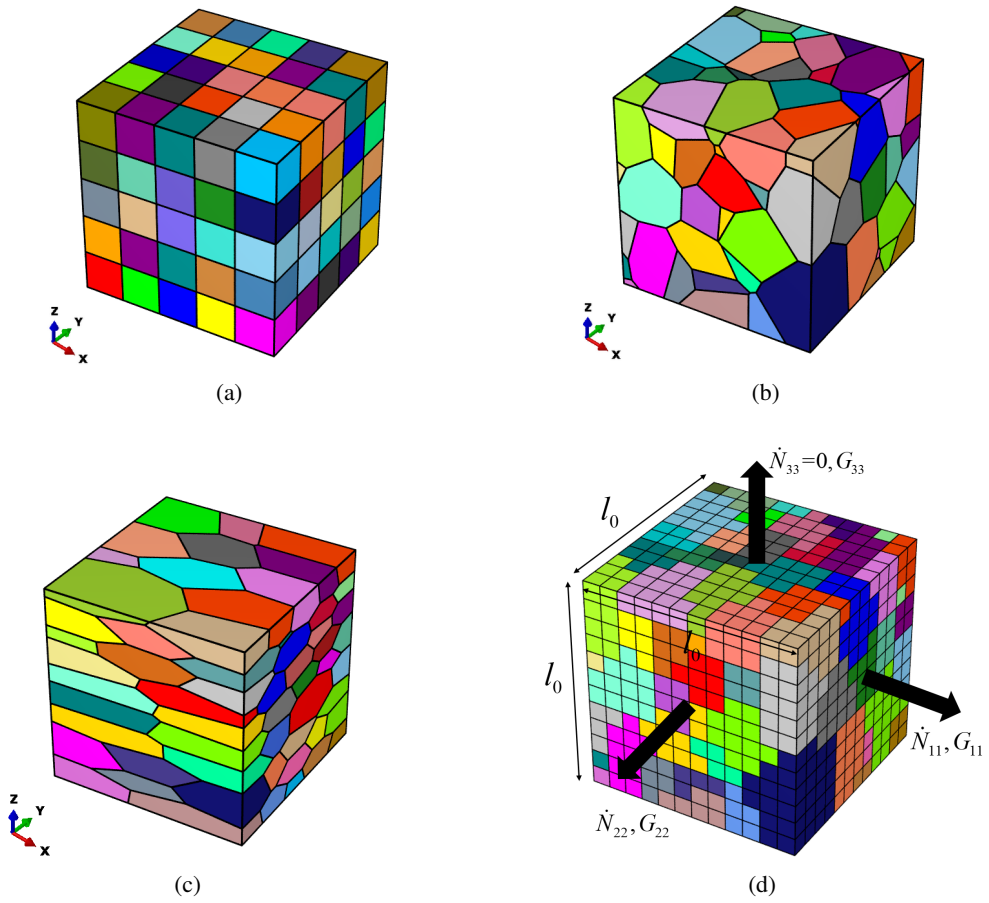

Figure 1 – Description of the polycrystalline aggregates: (a) cube morphology; (b) random morphology; (c) elongated morphology; (d) finite element mesh and the applied macroscopic loading.

where $\vec{N}$ is the unit vector normal to the localization band, equal to $(cos\theta, sin\theta)$, with angle θ ranging between 0 and $\pi/2$.

To investigate the influence of the crystallographic texture on the FLD predictions, three crystallographic textures are employed: random, cube ($\{001\} < 100 >$), and copper ($\{\bar{2}11\} < 111 >$). The (111) pole figures of the crystallographic textures with 125 orientations are plotted by the ATEX software [12] in Figure 2.

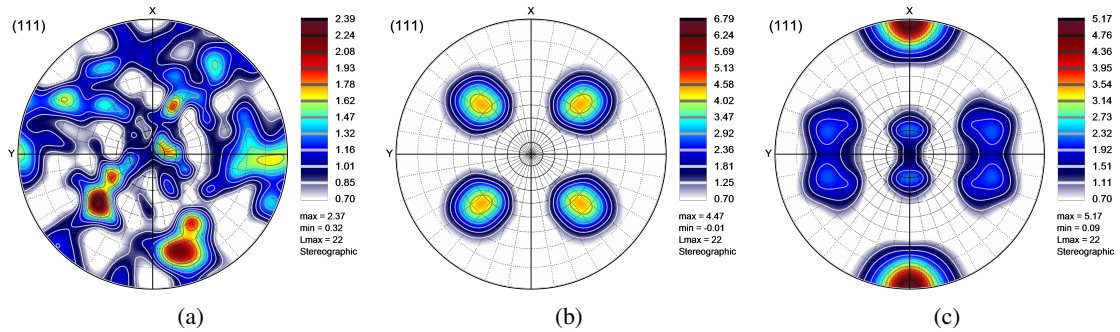

Figure 2 – (111) pole figures of the initial crystallographic textures with 125 orientations generated and plotted by the ATEX software: (a) random texture; (b) cube texture; (c) copper texture.

The elastic and isotropic hardening parameters used in the FLD predictions are listed in Table 1.

Table 1 – Elasticity and hardening parameters used in the FLD predictions.

E (GPa)	ν	τ_0 (MPa)	h_0 (MPa)	n
65	0.3	40	390	0.1

4 Results

The influence of crystallographic texture on formability is firstly examined. Figure 3 displays the forming limit diagrams covering the whole range of strain paths corresponding to the different grain morphologies. The results reveal that the crystallographic texture has a marginal effect on the predicted FLDs for the negative strain paths. This observation is consistent with classical trends found in the literature. This phenomenon can be attributed to the fact that, within this range of negative strain paths, forming limits are mainly dependent on the hardening parameters [9]. Moreover, in the case of the plane-strain tensile state ($\rho = 0$), various textures result in nearly identical limit strains, regardless of grain morphology. However, the right-hand side of the forming limit diagrams is highly influenced by the anisotropic behavior, which is mainly related to the initial texture and its evolution during plastic deformation. As a result, there is significant deviation on the right-hand side of FLDs obtained with different textures in Figure 3. Notably, the cube texture consistently offers the highest formability for $\rho > 0$, followed by random and then copper textures. Consequently, the cube texture can substantially enhance formability. These findings have also been corroborated in an earlier published paper [1], where the Taylor multiscale model and the M–K approach [13] have been employed to predict the formability limits of aluminum alloy sheets.

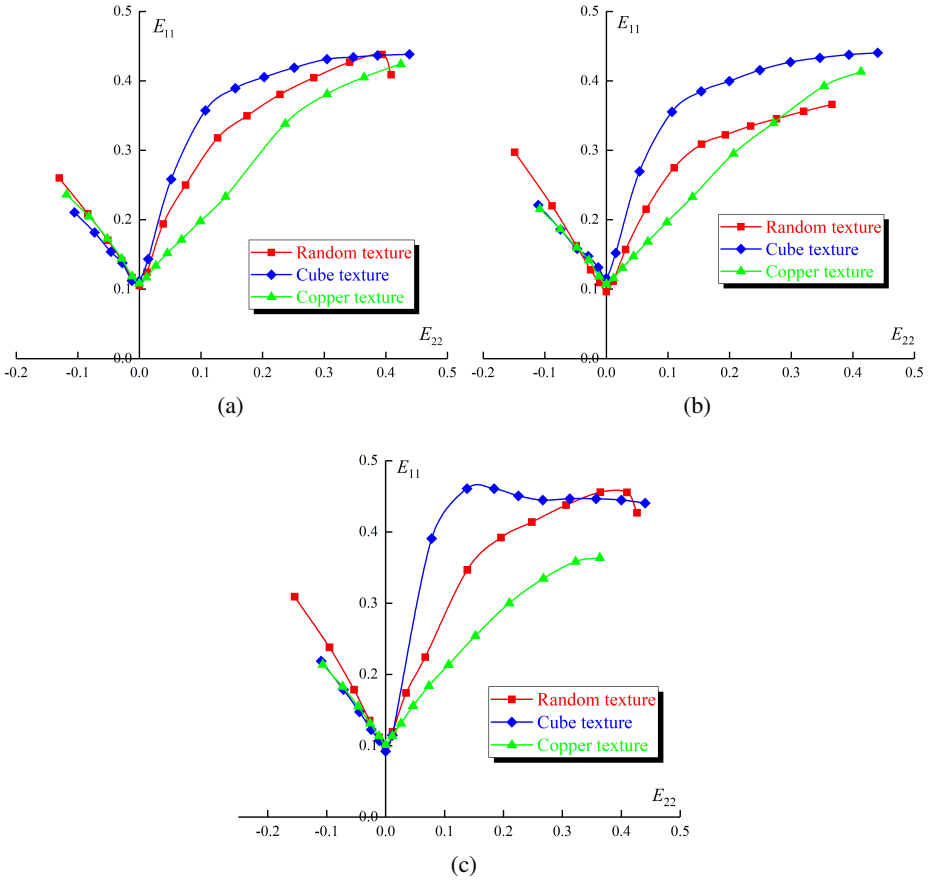

Figure 3 – Effect of crystallographic texture on the FLDs for: (a) cube morphology; (b) random morphology; (c) elongated morphology.

The effect of grain morphology on the predicted forming limits is then investigated, and the associated simulation results reported in Figure 4. It is clearly observed that nearly identical levels of forming limits are achieved for negative strain paths, while significant differences can be seen in the range of positive strain paths, owing to the use of various morphologies. This outcome can be attributed to the fluctuations in the micromechanical fields resulting from grain interactions and grain morphology. These fluctuations have a significant effect on plastic anisotropy and texture evolution, which in turn play an important role in the prediction of localized necking. Some conclusions are highlighted as follows:

- For random texture, the results suggest that elongated morphology leads to an improvement of formability, in comparison to cube and random morphologies.
- For cube texture, the predicted limit strains are nearly identical for cube and random morphologies, while elongated morphology yields higher limit strains in the range of positive strain paths.
- For copper texture, on the whole, the effect of grain morphology on the limit strains is almost indistinguishable.

Additionally, by comparison with Figure 3, it is evident that the effect of crystallographic texture on the limit strains is more important than that of grain morphology.

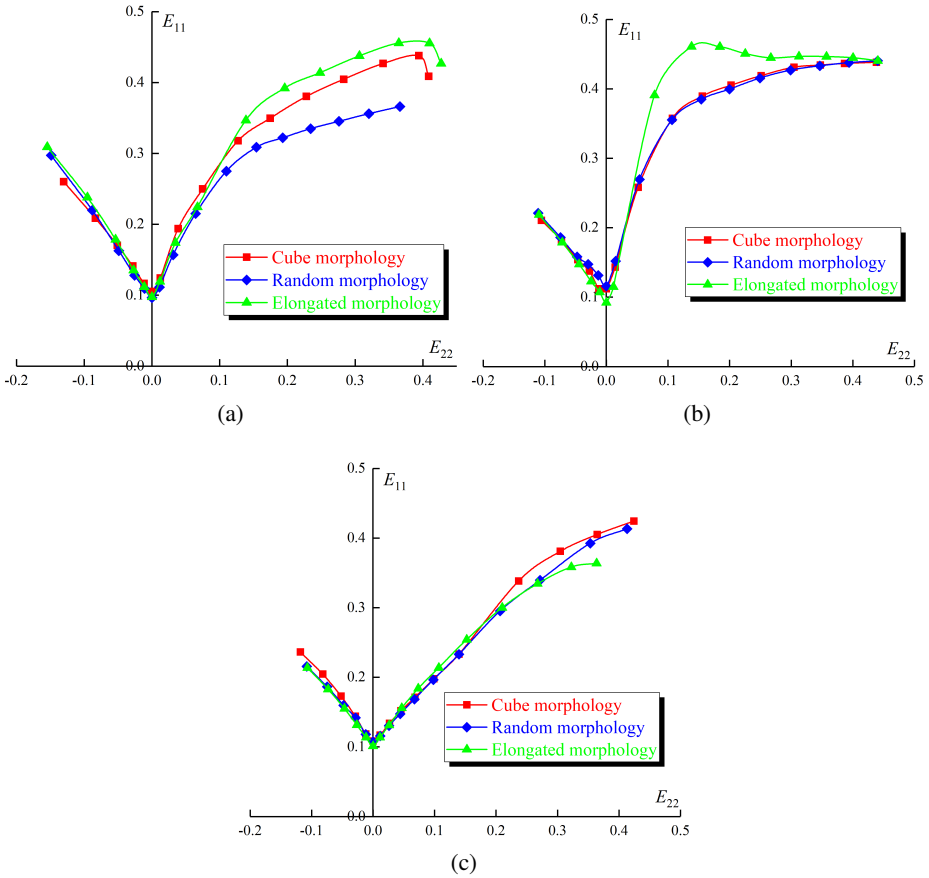

Figure 4 – Effect of morphological textures on the FLDs for: (a) random texture; (b) cube texture; (c) copper texture.

5 Conclusions

In this paper, the CPFEM has been coupled with the Rice bifurcation approach to analyze the effect of morphological and crystallographic textures on the ductility limits of thin metal sheets. The following conclusions are drawn from this study:

- The crystallographic textures (e.g., random, cube, and copper) can significantly influence the limit strains, especially in the range of positive strain-path ratios.
- The grain morphologies (e.g., cube, random, and elongated) can influence the predicted forming limits. According to the results of this study, this behavior is mainly linked to the type of initial

crystallographic texture.

- The effect of crystallographic textures on the forming limit predictions is more important than that of grain morphologies.

References

[1] K. Yoshida, T. Ishizaka, M. Kuroda, S. Ikawa. The effects of texture on formability of aluminum alloy sheets. Acta Mater, 55:4499–506, 2007.

[2] H. K. Akpama, M. Ben Bettaieb, F. Abed-Meraim. Localized necking predictions based on rate-independent self-consistent polycrystal plasticity: Bifurcation analysis versus imperfection approach. Int J Plast, 91:205–37, 2017.

[3] J.C. Zhu, M. Ben Bettaieb, F. Abed-Meraim, M.S. Huang, Z.H. Li. Coupled effects of crystallographic orientation and void shape on ductile failure initiation using a CPFE framework. Eng Fract Mech, 280:109121, 2023.

[4] J.C. Zhu, M. Ben Bettaieb, S. Zhou, F. Abed-Meraim. Ductility limit prediction for polycrystalline aggregates using a CPFEM-based multiscale framework. Int J Plast, 167:103671, 2023.

[5] G. Franz, F. Abed-Meraim, M. Berveiller. Effect of microstructural and morphological parameters on the formability of BCC metal sheets. Steel Res Int, 85:980–7, 2014.

[6] H. K. Akpama, M. Ben Bettaieb, F. Abed-Meraim. Influence of the yield surface curvature on the forming limit diagrams predicted by crystal plasticity theory. Lat Am J Solids Struct, 13(12): 2231–2250, 2016.

[7] O. Amelirad, A. Assempour. Experimental and crystal plasticity evaluation of grain size effect on formability of austenitic stainless steel sheets. J Manuf Process, 47:310–23, 2019.

[8] J. R. Rice. The localization of plastic deformation, 14th International Congress of Theoretical and Applied Mechanics, 207–20, 1976.

[9] J., Zhu, M., Ben Bettaieb, F., Abed-Meraim. Numerical investigation of necking in perforated sheets using the periodic homogenization approach. Int. J. Mech. Sci. 166:105209, 2020.

[10] R., Quey, P.R., Dawson, F., Barbe, Large-scale 3D random polycrystals for the finite element method: Generation, meshing and remeshing. Comput. Methods Appl. Mech. Eng. 200:1729–1745, 2011.

[11] J., Zhu, M., Ben Bettaieb, F., Abed-Meraim. Comparative study of three techniques for the computation of the macroscopic tangent moduli by periodic homogenization scheme. Eng Comput, 38:1365–1394, 2022.

[12] B. Beausir and J.-J. Fundenberger, Analysis Tools for Electron and X-ray diffraction, ATEX-software, www.atex-software.eu, Université de Lorraine - Metz, 2017.

[13] Z. Marciniak and K. Kuczyński. Limit strains in the processes of stretch-forming sheet metal. Int J Mech Sci, 9:609–20, 1967.